



PAPER

First-principles study of ZnO/Mg heterogeneous nucleation interfaces

RECEIVED
30 January 2018REVISED
1 March 2018ACCEPTED FOR PUBLICATION
5 March 2018PUBLISHED
21 March 2018Shu-Qing Yang¹ , Jun Du¹ and Yu-Jun Zhao²¹ School of Materials Science and Engineering, South China University of Technology, Guangzhou 510640, People's Republic of China² Department of Physics and Key Laboratory of Advanced Energy Storage Materials of Guangdong Province, South China University of Technology, Guangzhou 510640, People's Republic of ChinaE-mail: tandujun@sina.com**Keywords:** grain refining, magnesium alloy, polar surface, interfacial properties, first-principles calculation**Abstract**

The interfacial properties of ZnO(0001)/Mg(0001) and ZnO(000 $\bar{1}$)/Mg(0001) interfaces were investigated by theoretical calculations. It shows that the ZnO(000 $\bar{1}$)/Mg(0001) interface, with Mg atoms on the top of first layer O atoms of ZnO surface slab (OT site), has the lowest interface energy, and even lower than the interfacial energy of α -Mg/Mg melt (0.1 J m^{-2}). Considering interfacial energy and interfacial electronic properties, the calculated results and corresponding analysis support the heterogeneous nucleation potency of ZnO particles for α -Mg grains of magnesium alloys.

1. Introduction

Compared to other metal alloys, magnesium alloys have many advantages, including low density, excellent castability, high anti-radiation ability and easy to recycle or reuse, etc. So magnesium and its alloys are attractive and promising structural engineering alloys in modern industries [1–3]. Nowadays, magnesium alloys have been widely used in automobile and aerospace industries [4, 5]. It is well known that Mg-Al based alloys are the most important among a large number of commercial magnesium alloys, and they have been most widely used in industries [6]. However, wider applications of the Mg-Al based alloys were restricted owing to some disadvantages, including their poor formability and poor mechanical properties [7]. According to the experiment and theory, grain refinement can effectively ameliorate both the formability and mechanical properties of the metallic alloys [8]. Kinds of methods to refine cast Mg-Al based alloys have been developed, including superheating [9], the Elfinal process [10, 11] and carbon inoculation [12–14], etc. Among these approaches, carbon inoculation was regarded as a prospective grain refining method used in industries [8, 15]. However, the grain refining efficiency of carbon inoculation was easily disturbed by the solutes in Mg-Al melt, such as Fe and Mn. The potent nucleants in Mg-Al melt that treated by carbon inoculation was easily poisoned when Fe and Mn reacted with Al_4C_3 and Al-C-Fe(Mn)-rich compounds were produced [8, 16].

Up to now, the development of new grain refining methods for Mg-Al-based alloys has been paid attention by many researchers. Some oxides, including MgO [16–18], CaO [19] and ZnO [20, 21], were proved to effectively refine Mg-Al alloys. In 2008, using the E2EM model, Fu [20] *et al* identified that ZnO particles should be potential new grain refiners for magnesium alloys, and the ZnO particles could effectively refining pure Mg and Mg-Zn alloy according to experimental results. The results obtained by Saha [21] *et al* proved that ZnO grain refiner could refine AZ9E and Mg-9%Al binary alloys.

In order to refine the grain size of cast alloys by adding inoculants in the melt, the interfacial structure and interfacial energy between the nucleating particle and matrix crystal was the main determinant to judge the nucleating potency of a heterogeneous substrate. Using HRTEM and E2EM model, the detailed interfacial structure could be observed and analyzed [16, 17, 20]. However, it is still difficult to quantitatively assess the interfacial energy between one solid crystal and another solid crystal by experiment at present.

In the past decades, many researchers studied the interfacial characteristics between two different structures by the first-principles calculation, including interfacial atom structure, interfacial energy, electronic properties,

and charge transfer. These interfacial characteristics are crucial to study the refinement mechanism in metal alloys treated by inoculants, such as steel [22–24] and aluminum [25–27] alloys. In addition, charge transfer is an important characteristic to determine the stability and adsorption properties of the interface. Some experimental methods and calculation methods can be used to quantify the charge transfer amount [28]. Cai *et al* investigated the charge transfer of different heterostructures [28, 29] and small molecules adsorbed on monolayer InSe [30]. Recently, Ke *et al* studied the H-TiO₂@Ni(OH)₂ (core-shell) heterostructures [31] and proved that the core-shell morphology can be controlled by the introduction of defects in the interface. In the references [22] and [23], Yang *et al* studied the interfacial properties of ferrite/TiC and austenite(100)/LaAlO₃(100) models to judge whether TiC and LaAlO₃ could be potential nucleus for steel alloys, respectively. Xiong [24] *et al* investigated the effects of some alloying elements on ferrite/TiC interface, indicating that the introduction of Cr, Mo, W, Mn and V improves the stability of the ferrite/TiC interface. In Han's study [25], the calculated results show that the interfacial energy between AlB₂(0001) slab and Al(111) slab is clearly higher than that between Al melt and α -Al, indicating that AlB₂ is not effective refiner for Al alloys. Zhang *et al* [26] studied the interfacial properties between Al melts (liquid phase) and TiB₂ substrate (solid phase). Results show that five Al layers are apt to stack on the Ti-terminated TiB₂ slab and formed FCC Al(111) model. Deng *et al* [27] studied the effects of the doping Mg or Si atoms to the TiB₂/Al interface, indicating that the doping Mg or Si atoms will weaken the stability of the interface.

In recent years, the interfacial structures between heterogeneous nuclei and Mg matrix, such as Al₄C₃/Mg [32], Al₂CO/Mg [33], Al₂MgC₂/Mg [34] and MgO/Mg [35] have been widely investigated by first-principles calculations. Li *et al* investigated the interfacial structures of Al₄C₃/Mg models [32] and Al₂CO/Mg models [33] to expose the potential of Al₄C₃ and Al₂CO particles act as the refining nucleus for Mg alloys. Wang *et al* [34] investigated the interfacial properties of Al₂MgC₂(0001)/Mg(0002) slab. They found that the Mg-terminated Al₂MgC₂(0001)/Mg(0002) interface is the most stable and its interfacial energy lower than 0.1 J m⁻² (the interfacial energy of α -Mg/Mg melt), implying that Al₂MgC₂ could effectively refine the magnesium alloys. Song *et al* [35] studied three different MgO(1 $\bar{1}$ 1)/Mg(0001) interfaces. They found that Mg atoms in the melt are apt to grow along Mg-terminated MgO(1 $\bar{1}$ 1) surface with FCC site.

As ZnO has almost identical crystal structure to Mg by E2EM model, it is believed that ZnO can be potential nucleation of cast magnesium alloys [36, 37]. Some researchers proved that ZnO particles could effectively refining Mg-Zn alloy [20] and Mg-Al alloy [21] by experiment. However, the deep theoretical analysis on the ZnO/Mg interface has not been studied yet. To analyze the nucleation potency of ZnO particles for α -Mg grain in theory, further studies of the atomic structure and the interfacial energy of ZnO/Mg interface are required. The first-principles calculation is well established for calculating the interfacial properties between two different structures. In this work, the surface energies of ZnO(0001) slab and ZnO(000 $\bar{1}$) slab were studied. The interfacial energies and electron structures of ZnO(0001)/Mg(0001) and ZnO(000 $\bar{1}$)/Mg(0001) interfaces are systematically investigated with four different stacking-site models, including HCP, MT, OT and FCC sites. The heterogeneous nucleation potency of ZnO particles for cast magnesium alloys were also analyzed.

2. Computational methods

In this work, the VASP (Vienna *ab initio* simulation package) that based on the DFT (density of functional theory) [38], was employed to calculate. In all calculations, we used PAW (projected augmented wave) pseudopotentials and a plane-wave basis set [39]. The GGA (generalized gradient approximation) with the PBE (Perdew-Burke-Ernzerhof) [40] functional was opted as the exchange-correlation functional in this work. 450 eV was opted as the plane-wave cutoff energy. The Brillouin zone were selected as $15 \times 15 \times 9$, $15 \times 15 \times 1$ and $15 \times 15 \times 1$ for the bulk, slab and interface calculations, respectively. The vacuum thickness was set to 16 Å. The structures were fully relaxed until the forces on each atom are less than 5 meV/Å.

3. Convergence test

3.1. Bulk parameter

It is well known that Mg bulk is a hexagonal close-packed structure, and the experimental lattice constants are $a = 3.209$ Å and $c = 5.210$ Å [36]. The calculated lattice parameters are $a = 3.205$ Å and $c = 5.143$ Å, which are in agreement with the experimental values above. For the ZnO phase with a space group symmetry P63mc (186), the experimental values are $a = 3.250$ Å and $c = 5.207$ Å [37]. The calculated lattice parameters are $a = 3.284$ Å and $c = 5.258$ Å, which also in line with the experimental values. The used constants are precise enough to ensure the accuracy of this work according to the calculated results.

Table 1. Atom layer dependence of the surface energy of the Mg(0001) slab.

Atom layers (n)	3	5	7	9	11	13
Surface energy (J m ⁻²)	0.580	0.558	0.550	0.560	0.557	0.556

3.2. Surface properties

To ensure the Mg(0001), ZnO(0001) and ZnO(000 $\bar{1}$) slabs that used are suitable to this work, we have carried out convergence tests on these surface slabs prepared for further studies. The convergence calculation of Mg(0001) slab was carried out according to Ref. [41].

The surface energy of Mg(0001) slab were estimated according to the equation as follows:

$$E_{surf}(N) = \frac{1}{2A}(E_{tot} - nE_{Mg}^{bulk}) \quad (1)$$

where, E_{surf} is the surface energy of the N -layer slab; E_{tot} is the total energy of the Mg(0001) slab, E_{Mg}^{bulk} is the chemical potential of per Mg atom in the Mg bulk; n is the number of Mg atoms in the Mg(0001) slab; A is the surface area of Mg(0001) surface. The entropy and PV terms could be neglected when the system under the condition of 0 K temperature and typical pressures. As shown in the table 1, seven-atomic-layer Mg(0001) slab is sufficient convergence to be suitable for the calculation.

ZnO crystal does not have a center of inversion. It breaks the fewest interatomic bonds when the ZnO crystal is cleaved along (0001) and (000 $\bar{1}$) crystallographic planes, thus two opposite surfaces are formed, i.e., the Zn cation surface for the (0001)-Zn-terminated slab and the O anion surface for the (000 $\bar{1}$)-O-terminated slab. The ZnO(0001) and ZnO(000 $\bar{1}$) surfaces should be a polar surface since they both have a dipole moment in the repeat unit perpendicular to the surfaces, and the atoms in the cell are asymmetric along the c axis [42, 43]. Noguera [43] deemed that the characteristics of the charge distribution in the structure determines the stability of a compound surface. Wander *et al* [44] studied the ZnO polar surfaces by the first principles calculation, and found that the polar surfaces are stabilized when 0.17 electrons have transferred between the (0001)-Zn and the (000 $\bar{1}$)-O surfaces. In order to simulate the tricky polarized system, the bottom surface was passivated by pseudo-H atom as suggested by [45–48]. The artificial atom with 1/2 nuclear charge was added for each O-anion-outmost atom at O-terminate slab, and the artificial atom with 3/2 nuclear charge was added for each Zn-cation-outmost atom at Zn-terminated slab [45, 46].

The percentage changes of interlayer space for ZnO(0001) and ZnO(000 $\bar{1}$) surfaces after full relaxation are shown in table 2. There are obvious relaxations in the outmost three atomic layers of ZnO(0001) and ZnO(000 $\bar{1}$) surfaces. The changes of the interlayer space are not obvious between the bottom surfaces passivated by pseudo-H. For both ZnO(0001) and ZnO(000 $\bar{1}$) surfaces, the relaxations of interlayer distance were converged when $N \geq 18$ (not include the pseudo-H atom layer). Accordingly, we calculated the properties of ZnO surfaces and ZnO/Mg interfaces by using the 18 atomic layers for ZnO(0001) and ZnO(000 $\bar{1}$) surfaces that passivated by pseudo-H atoms.

According to the convergence test of Mg slabs and ZnO slabs (passivated by pseudo-H atom), the slabs for the further calculation are shown in figure 1.

3.3. Stabilities of ZnO surfaces

As the ZnO(0001) and ZnO(000 $\bar{1}$) surfaces are passivated by pseudo-H atom, the surface energies of ZnO(0001) and ZnO(000 $\bar{1}$) can be given by [47, 48]:

$$\sigma = \frac{1}{A}[E_{ZnO+H}^{slab} - n_O\mu_O - n_{Zn}\mu_{Zn} - n_{H_i}\mu_{H_i} - A\sigma_{bot}^{pass}] \quad (2)$$

where E_{ZnO+H}^{slab} is the total energy of the slab (its bottom side passivated by pseudo-H atom), n_i is the number of O(Zn) atoms in the slab, μ_i is the chemical potential of O(Zn) atom, n_{H_i} is the number of pseudo-H atom, μ_{H_i} is the chemical potential of pseudo-H that fractional charge, i refers to O or Zn atom, A is the area of the surface, and σ_{bot}^{pass} is the surface energy of the passivated bottom surface. The entropy and PV terms could be neglected under the condition of 0 K temperature and typical pressures. The chemical potentials μ_O and μ_{Zn} are constrained by the ZnO bulk as follows since the models meet stoichiometry:

$$\mu_O + \mu_{Zn} = \mu_{ZnO}^{bulk} \quad (3)$$

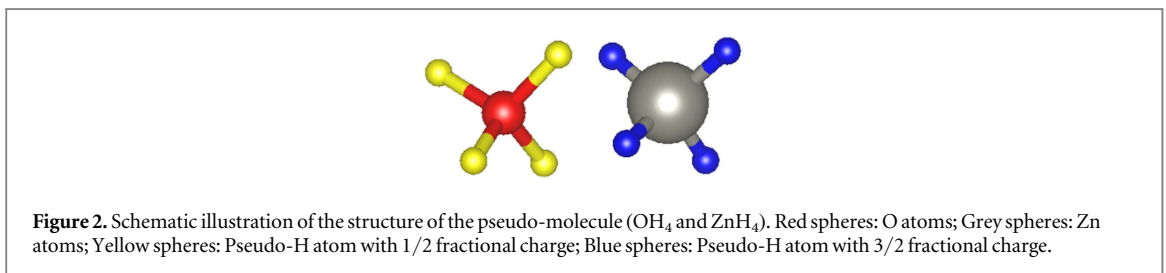
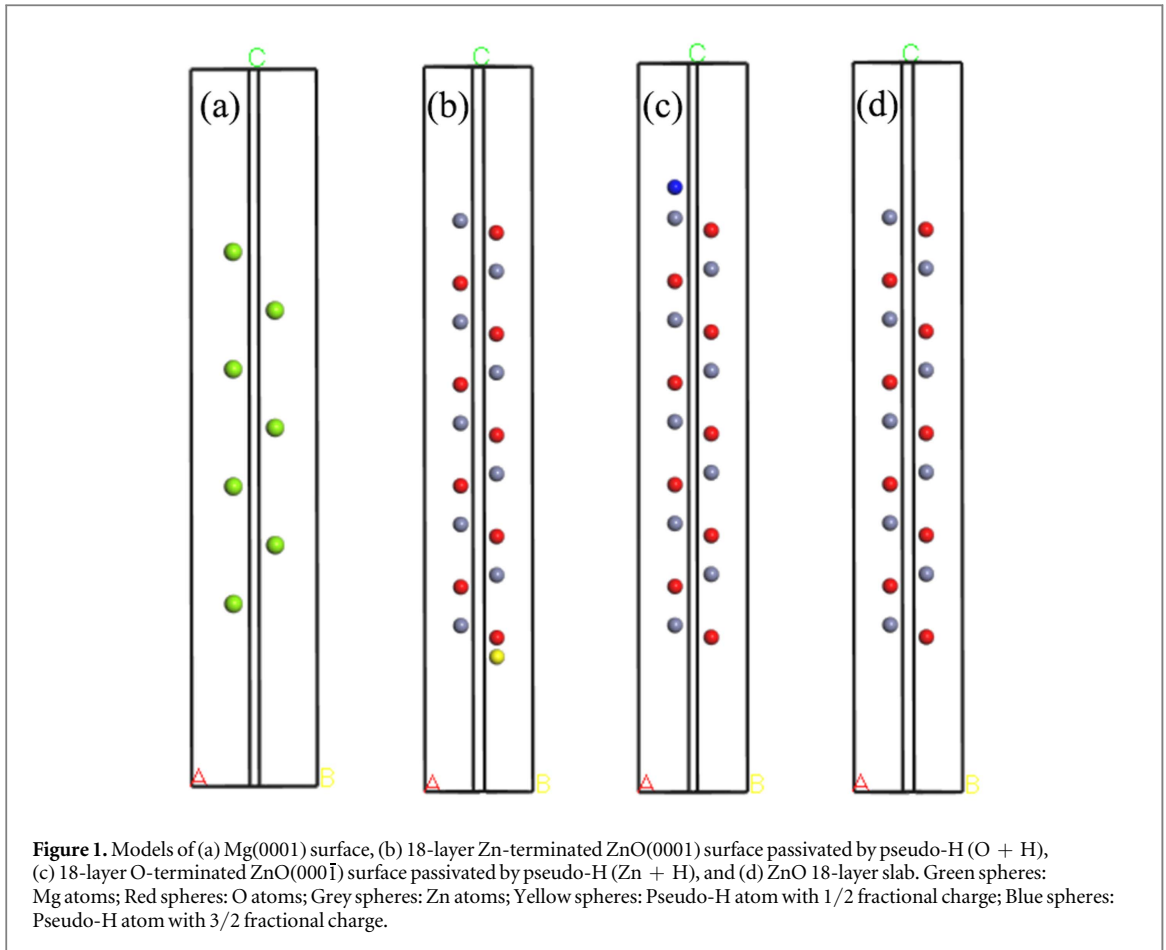
μ_{ZnO}^{bulk} where is the total energy of ZnO in a primitive bulk cell.

Based on formula (2) and (3), the surface energy of (0001) surface and (000 $\bar{1}$) surface is given by:

$$\sigma = \frac{1}{A}[E_{ZnO+H}^{slab} - n\mu_{ZnO}^{bulk} - n_{H_i}\mu_{H_i} - A\sigma_{bot}^{pass}] \quad (4)$$

Table 2. Interlayer distance perpendicular to the ZnO(0001) and ZnO(000 $\bar{1}$) surfaces, in terms of absolute distance and as a percentage of the respective bulk spacing(%)

Slab thickness(n)											
ZnO(0001) surface (O + H)						ZnO(000 $\bar{1}$) surface (Zn + H)					
Interlayer	14	16	18	20	22	Interlayer	14	16	18	20	22
$\Delta d_{H0.5-O}$	5.055	4.799	4.970	4.996	5.021	$\Delta d_{H1.5-Zn}$	1.337	1.292	1.247	1.284	1.234
Δd_{2-3}	-1.088	-0.448	-0.904	-0.773	-0.755	Δd_{2-3}	5.852	5.994	5.723	5.860	5.903
Δd_{3-4}	0.339	-0.087	0.207	0.181	0.086	Δd_{3-4}	0.032	-0.070	-0.132	-0.060	-0.193
Δd_{4-5}	4.298	4.423	4.696	5.026	5.010	Δd_{4-5}	4.713	4.871	4.154	4.897	4.461
Δd_{5-6}	0.501	0.140	0.282	0.221	0.107	Δd_{5-6}	0.162	0.105	0.019	0.080	-0.064
Δd_{6-7}	2.021	0.840	3.371	3.737	3.844	Δd_{6-7}	3.575	4.199	3.191	4.188	3.638
Δd_{7-8}	1.051	0.804	0.489	0.402	0.300	Δd_{7-8}	0.388	0.297	0.075	0.201	0.043
Δd_{8-9}	-0.104	-2.017	1.987	2.640	2.949	Δd_{8-9}	1.969	3.473	2.348	3.284	3.018
Δd_{9-10}	1.585	1.066	0.827	0.664	0.471	Δd_{9-10}	0.776	0.524	0.150	0.241	0.107
Δd_{10-11}	-2.902	-2.577	0.602	1.611	1.989	Δd_{10-11}	-1.088	2.073	1.627	2.513	2.332
Δd_{11-12}	2.442	1.731	1.203	0.925	0.728	Δd_{11-12}	1.924	0.909	0.338	0.302	0.150
Δd_{12-13}	-5.489	-4.255	-1.505	0.258	1.097	Δd_{12-13}	-11.807	-1.344	0.542	1.869	1.578
Δd_{13-14}	5.224	2.063	1.729	1.247	0.985	Δd_{13-14}	5.822	2.046	0.733	0.523	0.343
Δd_{14-15}	-22.941	-8.511	-3.853	-1.803	-0.412	Δd_{14-15}	-47.281	-11.702	-2.228	0.773	1.097
Δd_{15-16}		4.843	2.462	1.749	1.307	Δd_{15-16}		5.944	1.842	0.845	0.557
Δd_{16-17}		-21.232	-6.683	-3.930	-2.195	Δd_{16-17}		-46.835	-12.041	-2.448	0.343
Δd_{17-18}			5.281	2.473	1.778	Δd_{17-18}			5.901	1.830	0.878
Δd_{18-19}			-23.916	-6.701	-4.255	Δd_{18-19}			-47.470	-12.436	-2.059
Δd_{19-20}				5.389	2.549	Δd_{19-20}				5.912	1.992
Δd_{20-21}				-24.082	-7.069	Δd_{20-21}				-47.457	-12.080
Δd_{21-22}					5.440	Δd_{21-22}					6.061
Δd_{22-23}					-24.502	Δd_{22-23}					-47.358



According to the reference [43], the pseudo chemical potential $\hat{\mu}_{H_i}$ can be given by a pseudo-molecule method:

$$\hat{\mu}_{H_i} = \frac{1}{4} [E_{tot}(\text{pseudo} - \text{molecule}) - \mu_i] \quad (5)$$

Where $E_{tot}(\text{pseudo-molecule})$ is the total energy of this pseudo-molecule (OH₄ or ZnH₄) shown in figure 2, μ_i is the chemical potential of O or Zn. The range of the O and Zn chemical potential can be derived as [32, 34, 35]:

$$\mu_i^{bulk} + \Delta H_f(\text{ZnO}) \leq \mu_i \leq \mu_i^{bulk} \quad (6)$$

Where the μ_i^{bulk} is the O (Zn) atom chemical potential of O₂ molecule (Zn bulk). $\Delta H_f(\text{ZnO})$ is the formation enthalpy of bulk ZnO at 0 K, which is given by $\Delta H_f(\text{ZnO}) = \mu_{\text{ZnO}}^{bulk} - \mu_{\text{Zn}}^{bulk} - \frac{1}{2}\mu_{\text{O}_2}^{gas}$, and the calculated value is -3.35 eV.

The results of PCP and sum of PCPs are shown in table 3. It can be seen that sum of PCPs is -5.477 eV, in line with earlier reports (-5.476 eV) [48].

Table 3. Pseudo chemical potential (PCP) versus μ_{O} and sum of PCPs for different pseudo molecules.

	PCP/eV	μ_{O} /eV	sum of PCPs/eV
Pseudo molecule (OH ₄)	-2.434	-7.82	-5.477
	-3.272	-4.47	
Pseudo molecule (ZnH ₄)	-3.043	-7.82	
	-2.205	-4.47	

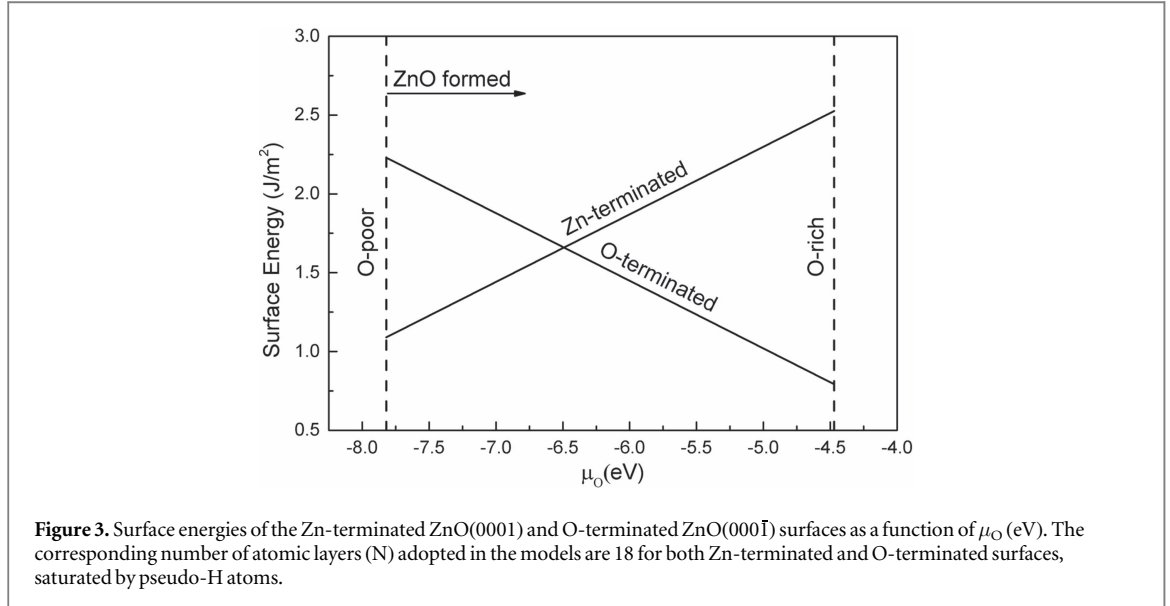


Figure 3. Surface energies of the Zn-terminated ZnO(0001) and O-terminated ZnO(000 $\bar{1}$) surfaces as a function of μ_{O} (eV). The corresponding number of atomic layers (N) adopted in the models are 18 for both Zn-terminated and O-terminated surfaces, saturated by pseudo-H atoms.

Pseudo chemical potential $\hat{\mu}_{H_i}$ is also defined as follows:

$$\hat{\mu}_{H_i} = \mu_{H_i} + \frac{A}{n_{H_i}} \sigma_{bot}^{pass} \quad (7)$$

So the surface energies of ZnO(0001) and ZnO(000 $\bar{1}$) surfaces are given by:

$$\sigma_{ZnO(0001)} = \frac{1}{A} [E_{ZnO(0001)}^{slab} - n_{ZnO}^{bulk} \mu_{ZnO} - n_{H_{O}} \hat{\mu}_{H_{O}}] \quad (8)$$

$$\sigma_{ZnO(000\bar{1})} = \frac{1}{A} [E_{ZnO(000\bar{1})}^{slab} - n_{ZnO}^{bulk} \mu_{ZnO} - n_{H_{Zn}} \hat{\mu}_{H_{Zn}}] \quad (9)$$

The surface energies of ZnO(0001) and ZnO(000 $\bar{1}$) slabs that calculated by equation (8) and equation (9) are shown in figure 3. The results agree well with the surface energy of ZnO nanoparticles tested by experiment [49]. The surface energy of Zn-terminated ZnO(0001) slab is lower than that of O-terminated ZnO(000 $\bar{1}$) slab at low chemical potential of O atom, indicating that ZnO(0001) slab is more stable under this condition. But the surface energy of O-terminated ZnO(000 $\bar{1}$) slab becomes lower when the chemical potential of O atom greater than -6.5 eV, indicating that ZnO(000 $\bar{1}$) slab is more stable as O chemical potential increases.

4. Interface

4.1. Interface structure of ZnO/Mg

On the basis of the surface stability analysis above, several different interface models of ZnO/Mg interfaces were built. The bottom surface of ZnO is passivated by fractional charged H. Both ZnO(0001) and ZnO(000 $\bar{1}$) slabs were employed to simulate the ZnO/Mg interfaces. Two different types of ZnO/Mg interfaces were defined as ZnO(0001)/Mg(0001) interface and ZnO(000 $\bar{1}$)/Mg(0001) interface, respectively.

A 7-layer Mg(0001) slab was placed on an asymmetric 18-layer ZnO(0001) slab and ZnO(000 $\bar{1}$) slab with passivated by 1-layer pseudo-H atom in a 1 × 1 cell, respectively. The interfacial distance was firstly set as 3 Å for ZnO(0001)/Mg(0001) interface and 2.8 Å for ZnO(000 $\bar{1}$)/Mg(0001) interface. An 8 Å vacuum was placed on

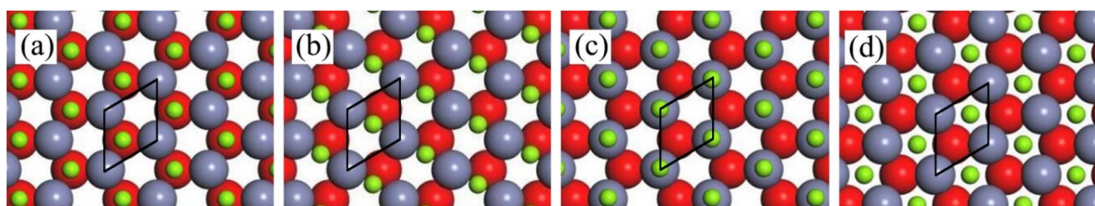


Figure 4. Four stacking sequences for ZnO(0001)/Mg(0001) interface before relaxation, (a) HCP, (b) MT, (c) OT, (d) FCC. Green spheres: Mg atoms; red spheres: O atoms; gray spheres: Zn atoms.

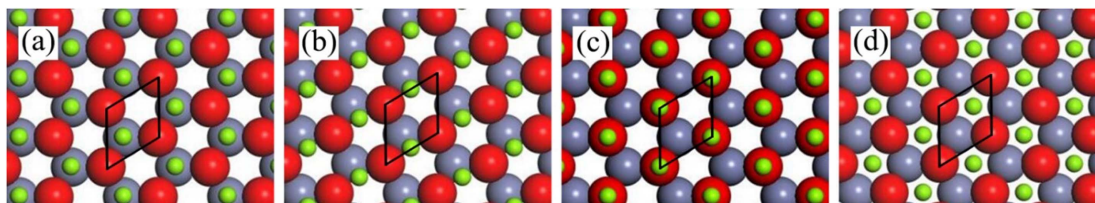


Figure 5. Four stacking sequences for ZnO(000 $\bar{1}$)/Mg(0001) interface before relaxation, (a) HCP, (b) MT, (c) OT, (d) FCC. Green spheres: Mg atoms; red spheres: O atoms; gray spheres: Zn atoms.

Table 4. Interfacial distance before relaxation (d_0) and after (d_1) and relaxed work of adhesion (W_{ad}). ‘passivated’ is the model of ZnO passivated by pseudo-H, ‘unpassivated’ is the ZnO slab not passivated by pseudo-H.

Interface	Stacking	$d_0(\text{\AA})$	passivated $d_1(\text{\AA})$	unpassivated $d_1(\text{\AA})$	passivated $W_{ad}(\text{J m}^{-2})$	unpassivated $W_{ad}(\text{J m}^{-2})$
ZnO(0001)/Mg(0001)	FCC	3.0	2.37	2.40	0.933	0.834
	HCP	3.0	2.25	2.24	1.059	0.984
	MT	3.0	2.25	2.24	1.033	0.964
	OT	3.0	2.27	2.24	0.957	0.898
ZnO(000 $\bar{1}$)/Mg(0001)	FCC	2.8	1.32	1.32	2.944	2.711
	HCP	2.8	1.96	1.96	3.065	2.869
	MT	2.8	1.33	1.32	2.917	2.698
	OT	2.8	1.97	1.97	3.161	2.946

both side of the ZnO/Mg interface slab. To counteract the misfit degree between ZnO slab and Mg slab and set up the ZnO/Mg interface, the softer Mg slab was extended by 2.41% to match the sizes of ZnO surface.

Four different stacking sequences were taken into account, including models HCP, MT, OT, and FCC. In the HCP model, the interfacial atoms of Mg slab are set at the *hcp* sites of ZnO slab, i.e., Mg atoms are set atop the second-outmost-layer atoms of ZnO slab. In the MT model, the interfacial Mg atoms are placed atop the middle of the outmost-layer atoms of ZnO slab. In the OT model, the Mg atoms are directly set atop the outmost-layer atoms of ZnO slab. In the FCC model, the interfacial atoms of Mg slab are set at the *fcc* sites of ZnO slab, i.e., Mg atoms are set atop the center of the outmost-layer atoms of ZnO slab. Therefore, eight kinds of interfacial models, as the figures 4 and 5 shown, were discussed in this study. In this work, all atoms were relaxed freely to their equilibrium sites.

4.2. Interface stability of ZnO/Mg

One of the main characteristics to study the interfacial property of ZnO/Mg is the W_{ad} (work of adhesion), which is the reversible-work needed to separate an interface into two free surfaces. The W_{ad} were estimated according to the equation as follows [32–34]:

$$W_{ad} = \frac{1}{A}(E_{ZnO}^{tot} + E_{Mg}^{tot} - E_{ZnO/Mg}^{tot}) \quad (10)$$

Where, E_i^{tot} is the total energy of the corresponding slab. Table 4 shows that the change of interfacial distance after relaxing and W_{ad} . The interfaces passivated and unpassivated by pseudo-H atom were compared and analyzed. The differences of d_1 between passivated and unpassivated interface models are all very small, and W_{ad} of passivated interface model are all bigger than unpassivated one. It can be seen that W_{ad} of the ZnO(000 $\bar{1}$)/Mg

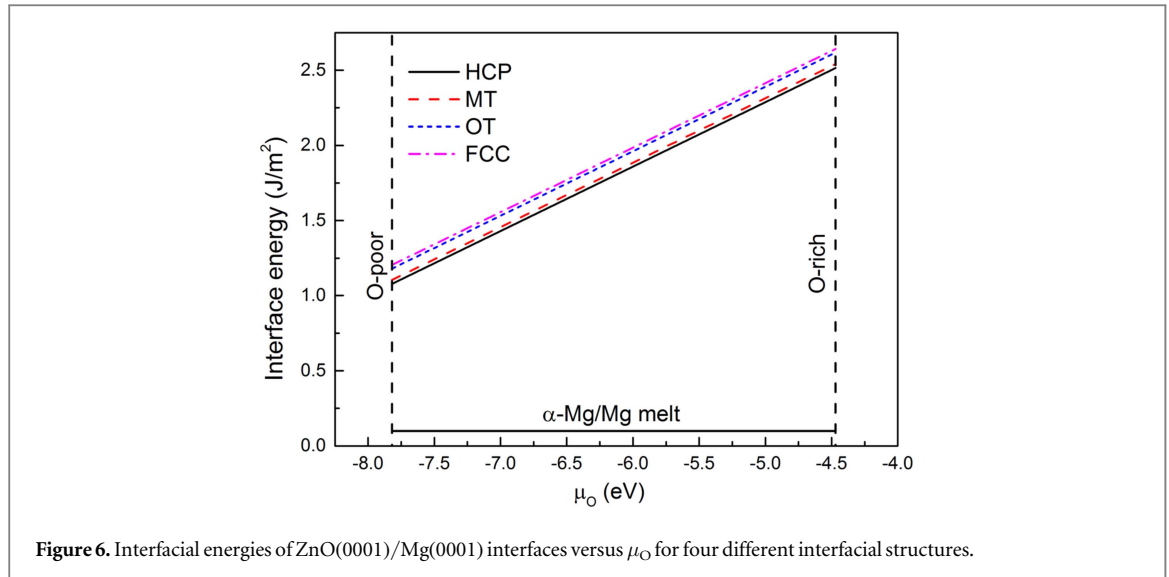


Figure 6. Interfacial energies of ZnO(0001)/Mg(0001) interfaces versus μ_{O} for four different interfacial structures.

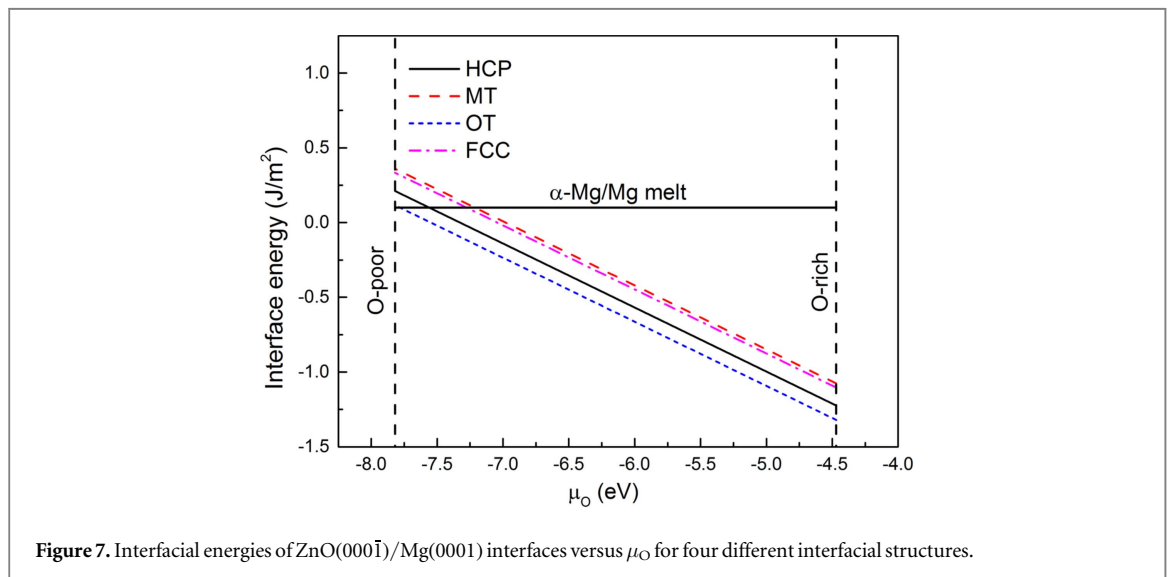


Figure 7. Interfacial energies of ZnO(0001̄)/Mg(0001) interfaces versus μ_{O} for four different interfacial structures.

(0001) interface is much bigger than W_{ad} of the ZnO(0001)/Mg(0001) interface and d_1 of ZnO(0001̄)/Mg(0001) interface is much smaller, these proves that interaction between the ZnO(0001̄)/Mg(0001) interfaces is stronger. In the ZnO(0001̄)/Mg(0001) interface models, W_{ad} of the OT stacking sequence is the greatest (3.161 J m^{-2}).

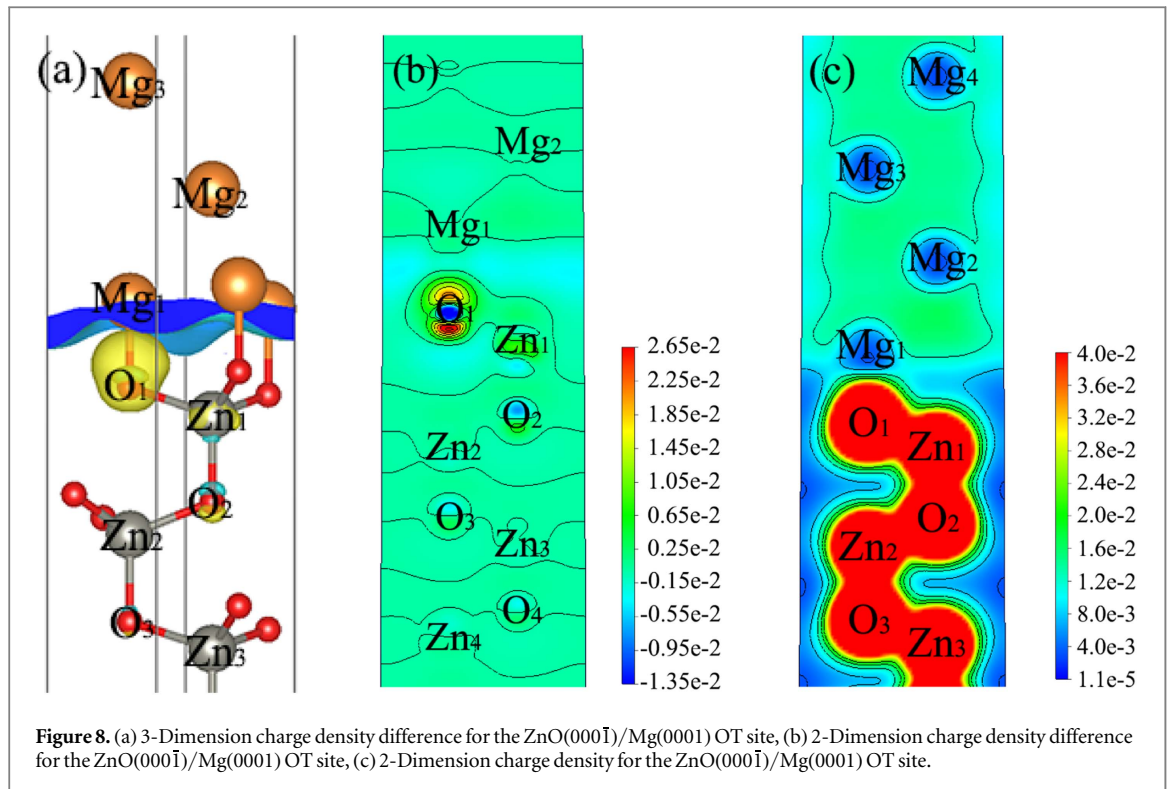
It is known that the interfacial energy is another important characteristic to study the interface property besides the W_{ad} . The interfacial structure is more stable of the smaller interfacial energy.

The interfacial energy of ZnO(0001)/Mg(0001) and ZnO(0001̄)/Mg(0001) interfaces are calculated by functions as follows [47, 48],

$$\gamma_{\text{ZnO}(0001)/\text{Mg}(0001)} = \frac{1}{A} [E_{\text{ZnO}(0001)/\text{Mg}(0001)} - n_{\text{O}}\mu_{\text{O}} - n_{\text{Zn}}\mu_{\text{Zn}} - n_{\text{Mg}}\mu_{\text{Mg}}^{\text{bulk}} - n_{\text{H}_\text{O}}\hat{\mu}_{\text{H}_\text{O}}] \quad (11)$$

$$\gamma_{\text{ZnO}(0001̄)/\text{Mg}(0001)} = \frac{1}{A} [E_{\text{ZnO}(0001̄)/\text{Mg}(0001)} - n_{\text{O}}\mu_{\text{O}} - n_{\text{Zn}}\mu_{\text{Zn}} - n_{\text{Mg}}\mu_{\text{Mg}}^{\text{bulk}} - n_{\text{H}_\text{Zn}}\hat{\mu}_{\text{H}_\text{Zn}}] \quad (12)$$

The interfacial energies of four different ZnO(0001)/Mg(0001) models are shown in figure 6. It shows that the interfacial energies of four different models are all higher than the interfacial energy between α -Mg and Mg melt (0.1 J m^{-2}) [50]. Figure 7 shows the interfacial energies versus μ_{O} for four different ZnO(0001̄)/Mg(0001) models. It indicates that the interfacial energies of HCP, MT and FCC sites are lower than 0.1 J m^{-2} over the partial range of μ_{O} , and the interfacial energy of OT model is almost lower than 0.1 J m^{-2} over the whole range of μ_{O} . Meanwhile, the W_{ad} of the ZnO(0001̄)/Mg(0001) OT model is the largest. Above all, the ZnO(0001̄)/Mg(0001) OT model is the most optimum structure.



4.3. Electronic structure

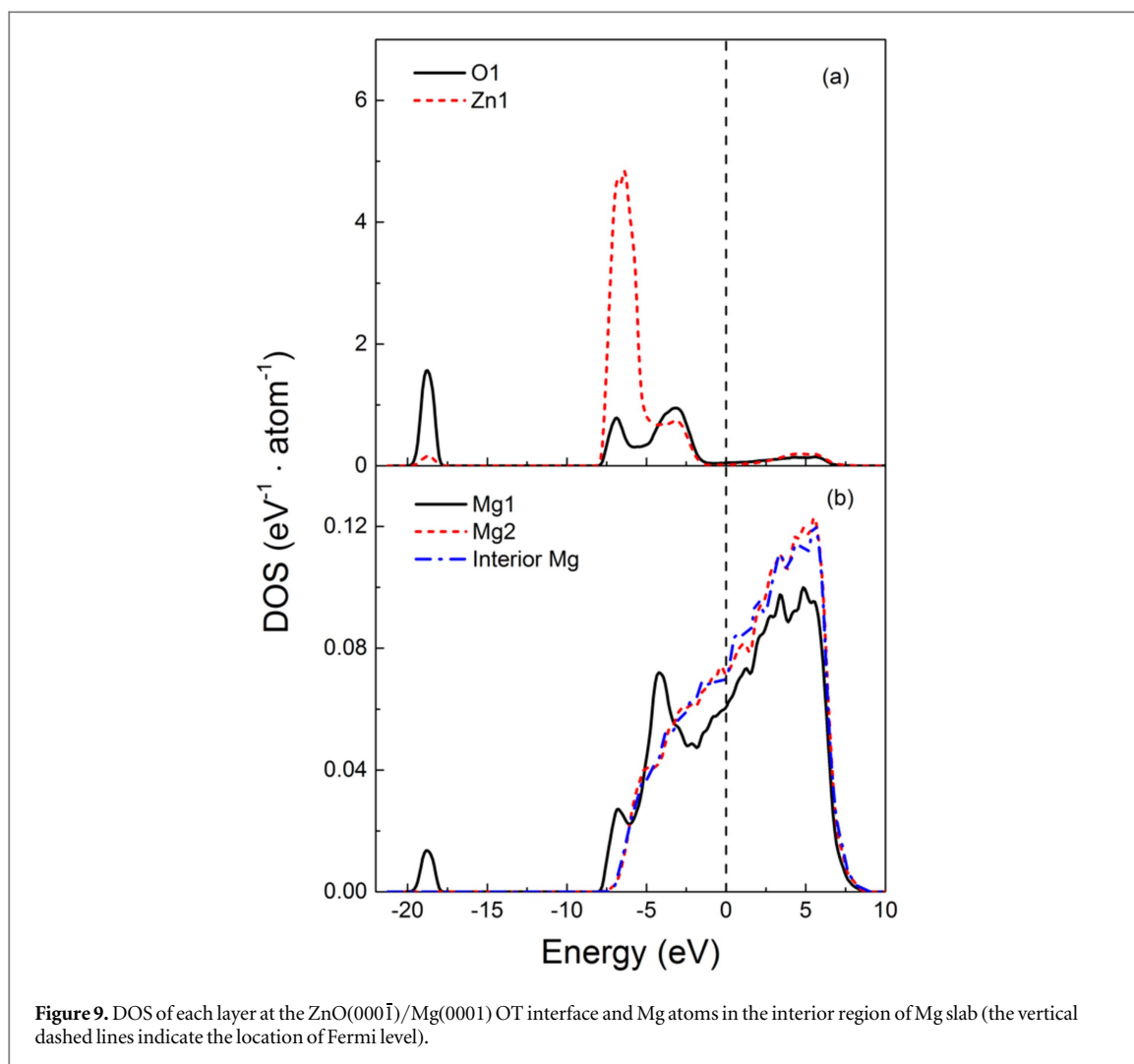
We can study the interface bonding between the ZnO(000 $\bar{1}$)/Mg(0001) OT interfacial structure by calculating the total charge density (TCD) and difference charge density (DCD). The charge density difference was calculated by the following formula [32, 34]:

$$\Delta\rho = \rho_{\text{ZnO}(000\bar{1})/\text{Mg}(0001)} - \rho_{\text{ZnO}(000\bar{1})} - \rho_{\text{Mg}(0001)} \quad (13)$$

Where $\rho_{\text{ZnO}(000\bar{1})/\text{Mg}(0001)}$ is the electron density of the ZnO(000 $\bar{1}$)/Mg(0001) slab, $\rho_{\text{ZnO}(000\bar{1})}$ and $\rho_{\text{Mg}(0001)}$ are the electron densities of ZnO(000 $\bar{1}$) and Mg(0001) slabs, respectively.

The 3-Dimension charge density difference is shown in figure 8(a), the yellow color means that electrons mainly accumulate around the O₁ atom. The 2-Dimension difference charge density is shown in figure 8(b). The charge density of O₁ atom is absolutely higher than that of Mg₁ atom shown in the picture (a) and (b), which indicates that ionic bonding exists between O₁ and Mg₁ atoms. The 2-Dimension total charge density is shown in figure 8(c), high charge density can be found between the metal-Mg atom and nonmetal-O atom, which indicates that covalent bond exists at the interface. As shown in the figure 8, it can be seen that the charge density rearrangements are mainly happened between the first two atomic layers in the interface region. In conclusion, the charge transfer near the interface is obvious, and it indicates that mixed ionic/covalent bond form between the Mg atom and O atom near the interface.

To further analyze the bonding in the interface region, the density of states (DOS) and layer partial density of states (PDOS) are needed. Figures 9 and 10 show that DOS and PDOS of several layers at the ZnO(000 $\bar{1}$)/Mg(0001) OT model and some Mg atoms of Mg slab, respectively. The valence electrons of O, Zn and Mg atoms for the DOS and PDOS calculations were O-2s²2p⁴, Zn-3d¹⁰4s², and Mg-3s², respectively. The A_n ($n = 1, 2, 3$) is layer-projected DOS and PDOS of the A atom in the n th-layer near the interface, for example, the Mg₂ means the layer-projected DOS of the Mg atom in the 2nd-layer. The interior Mg refers to the Mg atom in the center of Mg slab. As figure 9(b) shown, the DOS of Mg₁ is quite different from the DOS of Mg₂ and interior Mg, and the DOS of Mg₂ and interior Mg is similar. It shows that the DOS of Mg₂ and interior Mg both exhibit parabolic dispersion, indicating that the metallic bonding exists in the Mg slab. As figure 9 shown, it is found that the localized overlapping peaks exist from -20eV to -17.5 eV and -7.5 eV to -2.5 eV, indicating that strong electronic hybridization happened between Mg₁ and O₁ layer. As figure 10 shown, the partial density of states (PDOS) of these layers are analyzed to further disclose the electronic hybridization. There is slightly contribution from Mg₁-s and Mg₁-p peak around -18.75 eV below E_F to overlap with the corresponding O₁-s peak as shown in figure 3(b), indicating the interaction between Mg atom and O atom around the interface. The Mg₁-s peak around -6.25 eV and -4 eV below E_F overlaps with the corresponding O₁-p and Zn₁-d peak because of the highly localized O₁-p and Zn₁-d electrons. As above, the covalent bonding exists between the first O layer, first



Zn layer and first Mg layer, and it indicates that mixed ionic and covalent bonding exists between the first O layer and Mg layer. The combination of the ZnO(000 $\bar{1}$)/Mg(0001) OT interface is strong.

4.4. Heterogeneous nucleation analysis

It is well known that the results calculated at 0 K temperature by first principles calculation can explicate the phenomenon of experiment at high temperature for solid phase system [25]. According to the thermodynamic point of view, it is expected that the interface is more stable if its interfacial energy is lower. When the calculated interface energy between the solid particle and α -Mg grain is lower than that between Mg melt and α -Mg grain, it implies that the solid particle could be potential nucleus. As shown in figures 6 and 7, the interfacial energies of ZnO(0001)/Mg(0001) for four different interfacial structures is larger than 0.1 J m^{-2} with the range of μ_{O} , and that of ZnO(000 $\bar{1}$)/Mg(0001) interfaces is less than 0.1 J m^{-2} in a certain range of μ_{O} . From the interfacial energies and the work of adhesion, it is found that the ZnO(000 $\bar{1}$)/Mg(0001) interface is more stable than the ZnO(0001)/Mg(0001) interface. Moreover, the ZnO(000 $\bar{1}$)/Mg(0001) OT model is the most stable because its interface energy is the lowest. The results of charge density difference showed that the charge transfer near the ZnO(000 $\bar{1}$)/Mg(0001) OT interface is obvious. The strong electronic hybridization emerges between Mg₁ and O₁ layer near the interface according to the DOS and PDOS analysis. It indicates mixed ionic/covalent bond exists between Mg atom and O atom, and the combination of the ZnO(000 $\bar{1}$)/Mg(0001) OT interface is strong.

In addition to studying the interfacial properties between Mg slab and ZnO slab, the diffusion kinetics of single Mg adsorption on ZnO surfaces is important for the study of epitaxial growth of Mg on the ZnO nucleating substrate. Nishidate *et al* [51, 52] investigated the kinetics of Mg atom diffusing above ZnO polar surfaces. In our calculation, we used a slab containing $4 \times 4 \times 3$ ZnO unit cells and one side were passivated by pseudo-H atoms. The Brillouin zone was selected as $2 \times 2 \times 1$, the vacuum thickness was set as 20 Å. We considered three adsorption sites containing fcc site, hcp site and on-top site. Calculating the adsorption energy by the following formula:

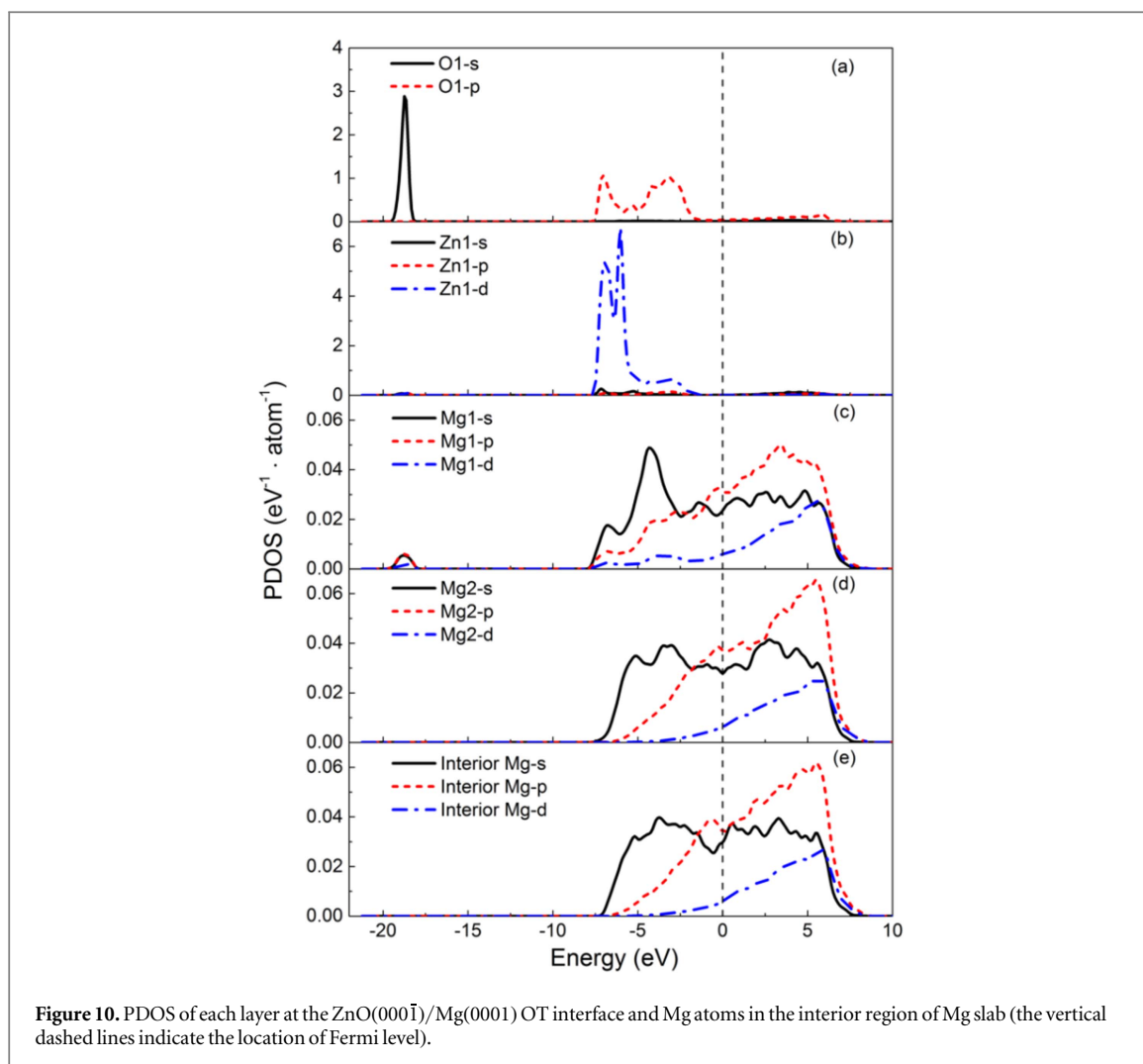


Table 5. The adsorption energies (E_{ad}) of Mg on ZnO polar surfaces.

E_{ad} (eV)			
adsorption site	fcc	hcp	on-top
Mg on ZnO(0001)surface	2.490	2.505	2.152
Mg on ZnO(000 $\bar{1}$)surface	-4.749	-4.261	-3.164

$$E_{ad} = E_{ZnO+Mg}^{tot} - E_{ZnO}^{tot} - \mu_{Mg} \quad (14)$$

E_{ZnO+Mg}^{tot} and E_{ZnO}^{tot} are the total energy of $4 \times 4 \times 3$ ZnO slab with and without Mg adsorption. μ_{Mg} is the chemical potential of Mg atom. The adsorption energies of Mg on ZnO polar surfaces are shown in table 5.

Our calculation results are in line with the results of the literature. The adsorption energies of Mg on the ZnO(0001) surface are positive, and the adsorption energies of Mg on the ZnO(000 $\bar{1}$) surface are negative. Mg atom adsorbed on fcc site and hcp site of ZnO(000 $\bar{1}$) surface are relatively stable because of the lower adsorption energy. Nishidate *et al* also analyzed the kinetics of single Mg diffusing above ZnO polar surfaces. It is found that Mg may diffuse with a relative low barrier (~ 0.5 eV) along the fcc-hcp-fcc zigzag path on the ZnO(0001) surface. However, its diffusion on ZnO(000 $\bar{1}$) surface is rather difficult due to its strong bonds with the surface-O atoms, which may be beneficial to the nucleation. In summary, the ZnO particles will act as effective nucleation substrate for α -Mg under the condition of low undercooling within ZnO(000 $\bar{1}$) surfaces.

5. Conclusions

We used the first-principles calculation to study ZnO/Mg heterogeneous nucleation interfaces, with assistant of pseudo-H atom passivation. Through a series of calculation and analysis, we get the following conclusions:

- (1) While the seven-atomic-layer Mg(0001) slab is well converged for the surface structural properties, more than 18 atomic layers (passivated by pseudo-H atoms) are required for the ZnO(0001) and ZnO(000 $\bar{1}$) slabs.
- (2) The interfacial energies of the ZnO(0001)/Mg(0001) slabs were all larger than 0.1 J m^{-2} , while the interfacial energies of ZnO(000 $\bar{1}$)/Mg(0001) slabs were less than 0.1 J m^{-2} (the interfacial energy of α -Mg/Mg melt) within a certain range of μ_{O} . The ZnO(000 $\bar{1}$)/Mg(0001) OT structure was the most stable, so Mg atoms are apt to stack atop outmost-O-layer atoms with an OT structure. The adsorption energies of Mg on ZnO(0001) surface are positive, and the adsorption energies of Mg on ZnO(000 $\bar{1}$) surface are negative.
- (3) Mixed ionic/covalent bond existed between Mg atom and O atom in the interface region of the ZnO(000 $\bar{1}$)/Mg(0001) OT model. The combination of the ZnO(000 $\bar{1}$)/Mg(0001) OT interface is strong. According to the geometry optimization, the work of adhesion and the interfacial energy, the ZnO particles are the potential heterogeneous nucleus for α -Mg grain from thermodynamics and kinetics.

Acknowledgments

This work was supported by the National Natural Science Foundation of China (51574127, 11574088) and Natural Science Foundation of Guangdong Province (2014A030313221).

ORCID iDs

Shu-Qing Yang  <https://orcid.org/0000-0003-2924-3260>

Jun Du  <https://orcid.org/0000-0002-1505-447X>

References

- [1] Yang Z, Li J P, Zhang J X, Lorimer G W and Robson J 2008 *Acta Metall. Sin. (Engl. Lett.)* **21** 313–28
- [2] Luo A A 2013 *Journal of Magnesium and Alloys* **1** 2–22
- [3] Wang X J et al 2017 *Journal of Materials Science & Technology* **34** 245–7
- [4] Kulekci M K 2008 *Int J Adv Manuf Technol* **39** 851–65
- [5] Du J D, Han W J and Peng Y H 2010 *Journal of Cleaner Production* **18** 112–9
- [6] Witik R A, Payet J, Michaud V, Ludwig C and Månson J A E 2011 *Composites Part A* **42** 1694–709
- [7] Byun J Y, Kwon S I, Ha H P and Yoon J K 2003 *Magnesium Alloys and Their Applications* (Weinheim: Wiley-VCH)
- [8] Ali Y, Qiu D, Jiang B, Pan F S and Zhang M X 2015 *Journal of Alloys and Compounds* **619** 639–51
- [9] Motegi T 2005 *Materials Science and Engineering: A* **413-414** 408–11
- [10] Song G L and Atrens A 1999 *Advanced Engineering Materials* **1** 11–33
- [11] Cao P, Qian M and StJohn D H 2004 *Scripta Materialia* **51** 125–9
- [12] Qian M and Cao P 2005 *Scripta Materialia* **52** 415–9
- [13] Kim Y M, Yim C D and You B S 2007 *Scripta Materialia* **57** 691–4
- [14] Yano E, Tamura Y, Motegi T and Sato E 2003 *Materials Transactions* **44** 107–10
- [15] StJohn D H, Easton M A, Qian M and Taylor J A 2012 *Metallurgical and Materials Transactions A* **44** 2935–49
- [16] Wang Y, Fan Z, Zhou X and Thompson G E 2011 *Philosophical Magazine Letters* **91** 516–29
- [17] Fan Z, Wang Y, Xia M and Arumuganathar S 2009 *Acta Materialia* **57** 4891–901
- [18] Men H, Jiang B and Fan Z 2010 *Acta Materialia* **58** 6526–34
- [19] Ali Y, Qiu D, Jiang B, Pan F S and Zhang M X 2016 *Scripta Materialia* **114** 103–7
- [20] Fu H M, Qiu D, Zhang M X, Wang H, Kelly P M and Taylor J A 2008 *Journal of Alloys and Compounds* **456** 390–4
- [21] Saha S and Ravindran C 2015 *International Journal of Metalcasting* **9** 33–42
- [22] Yang J, Zhang P F, Zhou Y F, Guo J, Ren X J, Yang Y L and Yang Q X 2013 *Journal of Alloys and Compounds* **556** 160–6
- [23] Yang J, Hou X, Zhang P F, Zhou Y F, Xing X L, Ren X J and Yang Q X 2014 *Computational and Theoretical Chemistry* **1029** 48–56
- [24] Xiong H H, Zhang H H, Zhang H N and Zhou Y 2017 *Journal of Iron and Steel Research, International* **24** 328–34
- [25] Han Y F, Dai Y B, Shu D, Wang J and Sun B D 2011 *Applied Surface Science* **257** 7831–6
- [26] Zhang H L, Han Y F, Dai Y B, Wang J and Sun B D 2012 *Journal of Physics D: Applied Physics* **45** 455307
- [27] Deng C, Xu B, Wu P and Li Q L 2017 *Applied Surface Science* **425** 639–45
- [28] Cai Y Q and Feng Y P 2016 *Progress in Surface Science* **91** 183–202
- [29] Cai Y Q, Zhang G and Zhang Y W 2015 *The Journal of Physical Chemistry C* **119** 13929–36
- [30] Cai Y Q, Zhang G and Zhang Y W 2017 *The Journal of Physical Chemistry C* **121** 10182–93
- [31] Ke Q Q, Guan C, Zhang X, Zheng M R, Zhang Y W, Cai Y Q, Zhang H and Wang J 2017 *Advanced Materials* **29** 1604164
- [32] Li K, Sun Z G, Wang F, Zhou N G and Hu X W 2013 *Applied Surface Science* **270** 584–9
- [33] Wang F, Li K and Zhou N G 2013 *Applied Surface Science* **285** 879–84
- [34] Wang H L, Tang J J, Zhao Y J and Du J 2015 *Applied Surface Science* **355** 1091–7
- [35] Song H Q, Zhao M and Li J G 2016 *Modern Physics Letters B* **30** 1650152

- [36] Walker C B and Marezio M 1959 *Acta Metallurgica* **7** 769–73
- [37] Kim Y, Page K and Ram S 2007 *Applied Physics Letters* **90** 101904
- [38] Rajagopal A K and Callaway J 1973 *Physical Review B* **7** 1912–9
- [39] Blöchl P E 1994 *Physical Review B* **50** 17953–79
- [40] Perdew J P, Burke K and Ernzerhof M 1996 *Phys Rev Lett* **77** 3865–8
- [41] Boettger J C 1994 *Physical Review B* **49** 16798–800
- [42] Tasker P W 1979 *J. Phys. C: Solid State Phys.* **12** 4977–84
- [43] Noguera C 2000 *J. Phys.: Condens. Matter* **12** R367–410
- [44] Wander A, Schedin F, Steadman P, Norris A, McGrath R, Turner T S, Thornton G and Harrison N M 2001 *Phys Rev Lett* **86** 3811–4
- [45] Meyer B and Marx D 2004 *Physical Review B* **69** 235420
- [46] Chen X, Huang D, Deng W J and Zhao Y J 2009 *Physics Letters A* **373** 391–5
- [47] Zhang Y O, Zhang J Z, Tse K F, Wong L, Chan C K, Deng B and Zhu J Y 2016 *Sci Rep* **6** 20055
- [48] Zhang J Z, Zhang Y O, Tse K F, Deng B, Xu H and Zhu J Y 2016 *Journal of Applied Physics* **119** 205302
- [49] Navrotsky A 2011 *Chemphyschem* **12** 2207–15
- [50] Jiang Q and Lu H M 2008 *Surface Science Reports* **63** 427–64
- [51] Nishidate K, Yoshizawa M and Hasegawa M 2008 *Physical Review B* **77** 035330
- [52] Nishidate K and Hasegawa M 2011 *e-Journal of Surface Science and Nanotechnology* **9** 199–205